



Synthesis of Schiff-Based Derivative as a Novel Corrosion Inhibitor for Mild Steel in 1 M HCl Solution: Optimization, Experimental, and Theoretical Investigations

Zenaa Ibraheem Jasim¹ · Khalid H. Rashid¹ · Khalida F. AL-Azawi² · Anees A. Khadom³

Received: 16 March 2023 / Revised: 25 May 2023 / Accepted: 13 June 2023 / Published online: 20 June 2023
© The Author(s), under exclusive licence to Springer Nature Switzerland AG 2023

Abstract

Due to the growing concern about corrosion problems caused by acidic attacks, the anticorrosive properties of synthetic corrosion inhibitor has been studied. The present work assessed the synthesis and inhibition performance of 3-((dicyclohexyl amino)methyl)-5-(4-((2-hydroxybenzylidene) amino phenyl)-1, 3, 4-oxadiazole-2(3H)-thione (DHOT) on the corrosion of mild steel in 1 M HCl solution through weight loss and electrochemical measurements. DHOT was characterized using FTIR and ¹H NMR measurements. Surface analysis was carried out using SEM and AFM. Chemical theoretical studies of DHOT were performed using density functional theory (DFT) calculations. Electrochemical measurement results showed that corrosion inhibition increased as inhibitor concentration increased, achieving a significant inhibition efficiency of 98.86% at optimum conditions. Polarization curves indicated that molecules of DHOT acted as a mixed-type inhibitor, and their adsorption process obeyed the Langmuir isotherm. Examination of corroded steel surface by SEM and AFM confirmed the adsorption of DHOT on metal surface. Chemical quantum calculations were used to determine the electronic properties of the DHOT and to explain inhibitor/metal surface interactions.

Keywords Corrosion inhibitor · Synthesis · Weight loss · Electrochemical · Quantum chemical

1 Introduction

Metal corrosion is one of the biggest problems facing the industry today. Despite its exceptional advantages, such as its superior mechanical capabilities and cost, low-carbon steel, one of the most common building materials, is very susceptible to corrosive ions [1–3]. Steel alloys have a tendency to react aggressively in acids, one of the most aggressive media. For this purpose, many methods including anodic and cathodic protection, anti-corrosion coatings, corrosion inhibitors, and others have been proposed

[4–6]. Corrosion inhibitors stand out as a promising strategy among all of these techniques. The right corrosion inhibitor is chosen based on important factors, including adsorption capacity, environmental friendliness, and affordability [7, 8].

The use of organic compounds with aromatic ring, π bond, and hetero-atoms (such as, nitrogen, phosphorus, sulphur, and oxygen atoms) is recommended as corrosion inhibitors [9, 10]. Commonly, organic compounds can adsorbed upon the steel surface either by the electrostatic interactions or bond formation through pi orbital and lone pair, consequently decrease the deterioration process [11, 12]. The adsorption of organic inhibitors is primarily influenced by a number of characteristics, including the electronic structure of the molecules, functional groups, steric factors, and electron density in orbits [13, 14]. Some organic corrosion inhibitors' harmful qualities and negative effects on the environment have tended to restrict their use. Consequently, recent studies have concentrated on the synthesis and employing brand-new, ecologically friendly inhibitors. The most environmentally friendly compounds are those with azole groups, such as thiadiazole, thiazole,

✉ Anees A. Khadom
aneesdr@gmail.com

¹ Department of Chemical Engineering, University of Technology, Iraq, Baghdad, Iraq

² Applied Chemistry Branch, Applied Science Department, University of Technology, Iraq, Baghdad, Iraq

³ Department of Chemical Engineering, College of Engineering, University of Diyala, Baqubah, Daiyla Governorate, Iraq

imidazole, and benzimidazole, which have corrosion-inhibiting action [15–18].

Nitrogen-containing derivatives has gained considerable attention in many industrial and chemical applications [19]. These derivatives have recently been described as a new class of metal corrosion inhibitors in several investigations due to the availability of their π -electrons of the $-C=N$ double bond, which can coordinate with metals to form a barrier between the metal and corrosive elements. Better inhibition performance is offered by inhibitors containing S, N, and O. Thio-derivatives of these compounds have been thoroughly researched for decades to prevent the corrosion of carbon steel in acidic conditions. To introduce these heteroatoms in organic structure, the design and synthesis of newly corrosion inhibitors can be achieved. Due to their strong efficiency at relatively low concentrations, synthesized organic inhibitors are among the best approaches. Typically, molecules containing at least one active heteroatom allow them to adhere to the surface of the metal [20, 21]. There has been a lot of study lately that has concentrated on the synthesis of Schiff-based derivatives as corrosion inhibitors. El Aatiaoui et al. [22] reported a yield of two new Schiff bases with an efficiency of more than 90%. Sayed and El-Lateef [23] conducted a thorough analysis of heterocyclic compounds under various corrosive circumstances. Donor–acceptor interactions are a key component of the inhibitor’s adsorption mechanism, and nitrogenous heterocyclic compounds frequently perform as mixed-type inhibitors. The maximum corrosion inhibition efficiency was 96.7% at 303 K and 500 ppm inhibitor concentration, according to Vranda Shenoy et al. evaluation of the inhibitory action of imidazopyridine derivatives on the corrosion of mild steel in HCl acid in their study published in 2014 [24].

The synthesis and characterization of N, S, and O containing organic derivatives family are of particular interest to biological, medicinal, and pharmaceutical potential. The application and comprehension of their inhibitive mechanism as a novel effective corrosion inhibitor was carried out in order to continue the search for another highly important activity of these hetero-compounds. Therefore, the present work aims to synthesis, characterization, and testing the corrosion inhibitory effect of 3-((dicyclohexyl amino) methyl)-5-(4-((2-hydroxybenzylidene) amino phenyl)-1,3,4-oxadiazole-2(3H)-thione (DHOT) against low-carbon steel corrosion in 1 M HCl. The newly corrosion inhibitor was characterized using FTIR and NMR. The weight loss tests were performed and optimized according to Doehlert experimental design as a function of temperature and DHOT concentration. Then, electrochemical,

morphological and other important tests were conducted in optimal conditions.

2 Methodology

2.1 Materials and Chemicals

All chemical material used in the reactions of the study was obtained from Sigma-Aldrich Chemicals Ethanol absolute (99.99%), 4-aminoethyl benzoate (99%), hydrazine hydrate (80%), potassium hydroxide (99%), carbon disulfide (99%), formaldehyde (37%) except glacial acetic acid from BDH (99%), dicyclo hexyl amine from MERCK-Schuchardt (95) and salicylaldehyde from CDH (99%).

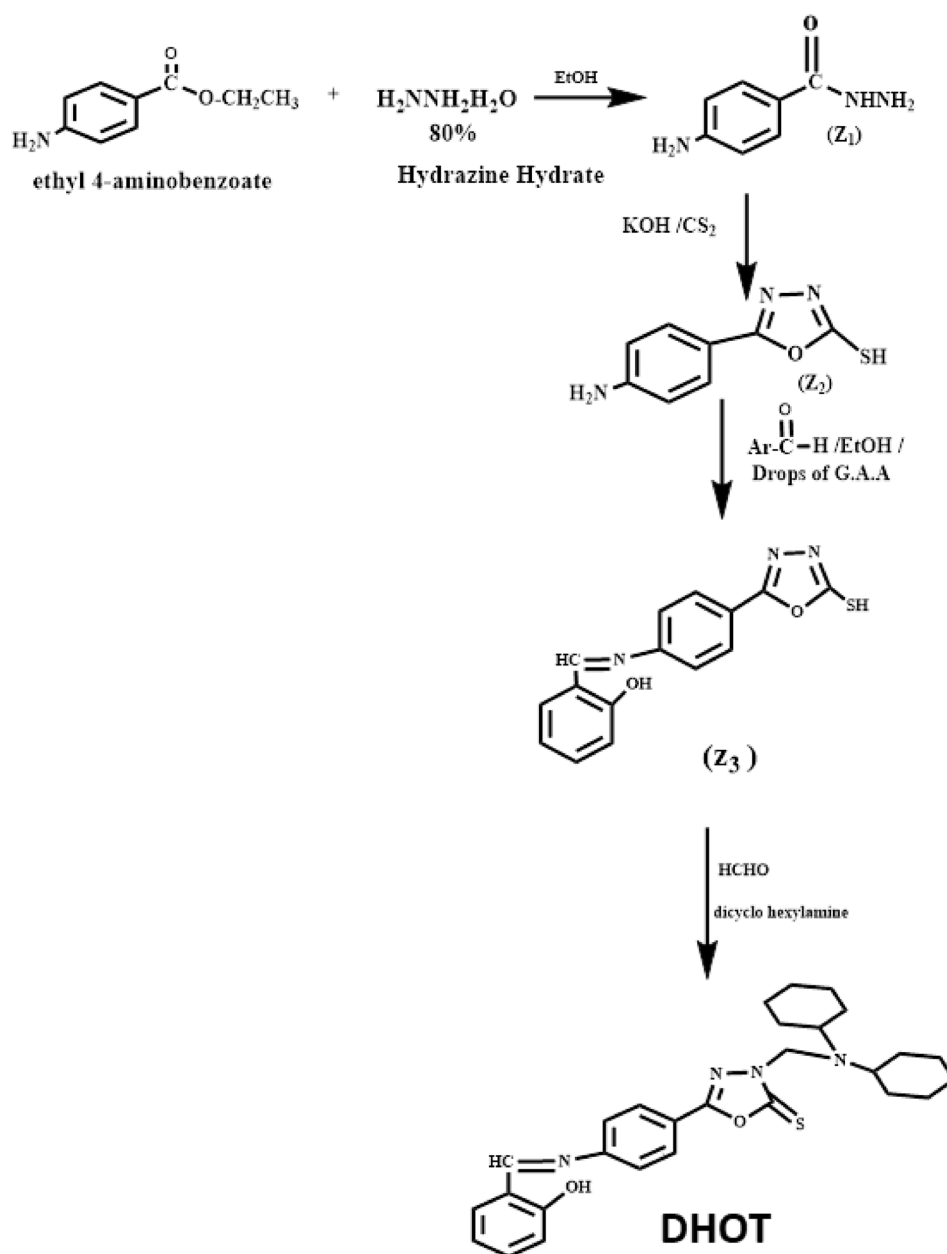
Corrosion experiments were achieved on mild steel samples Mild steel compositions were as follows: Carbon 0.08%, Manganese 0.2%, Silicon 0.03%, Phosphorous 0.01%, Aluminum 0.02%, Chromium 0.05%, and remainder is iron. The dimensions of rectangular steel were 3 cm \times 1 cm \times 0.1 cm. Before immersion in the corrosive solution, steel samples were cleaned with 800–1500 sand paper and rinsed in distilled water before each test. The entire experimental was given in detail in our previous papers [4–6] described, including the cleaning steps. The hydrochloric acid (37% wt) was diluted to make the corrosive 1 M HCl solution. To ensure an adequate level of repeatability, all measurements were taken twice.

2.2 FTIR, UV-Vis, and ¹HNMR Measurements

KBr Disc FTIR spectra were taken using SPEACTUM-65 in the range of 4000–400 cm^{-1} . In optimal conditions, the FTIR of the synthesized DHOT and the corrosion products from metal surfaces in the presence of DHOT were studied. The UV-spectrophotometer was used to take UV-Vis readings (Shimadzu, Japan, UV-1800). A UV spectrum for optimum temperature and concentration of DHOT in 1 M HCl was taken before and after the samples were immersed for 3 h. In addition, BRUKER instruments (USA) are used for ¹HNMR spectroscopic studies of DHOT.

2.3 Synthesis of DHOT

A Heterocyclic compounds are cyclic compounds plus one carbon atom that contain other atoms like nitrogen, oxygen, and sulfur [25]. It can be in the aromatic or long-chain carbon configuration. The synthesis procedure of DHOT included the formation of four intermediate compounds (symbolized as z1–z3) until reaching the final product. DHOT was synthesized according to a regular Mannich reaction [25]. A schematic path was shown in Fig. 1.

Fig. 1 Schematic synthesis of DHOT

2.3.1 Synthesis of 4-amino Benzoic Hydrazide (z₁)

4.9557 g of solid 4-amine ethyl benzoate (Sigma-Aldrich, USA) was dissolved in 25 ml of ethanol (Sigma-Aldrich, USA). Later, 20 ml of (80%) hydrazine hydrate was added gradually. After 8 h of refluxing, the mixture was allowed to cool to room temperature until the second day. A white crystals was observed and the formed sediment was filtered and recrystallized with ethanol [26]. 70.19%, 225–227 °C, white, ethanol, and C₇H₉O N₃ were the yield, melting point, color, recovery solvent, molecular formula of z₁, respectively.

2.3.2 Synthesis of 5 (4-amino phenyl) 1, 3, 4 Oxadiazole-2thiol (z₂)

The compound z₁ (1 g, 0.006 mol) was dissolved in 10 ml of ethanol and added to a solution containing (5%) of KOH. A 5 ml of carbon disulfide was added to the mixture, and it was refluxed for 8 h. The residue was then dissolved in water and acidified by adding 10% HCl to the solution (pH=3) [27]. 80%, 226–228 °C, yellow, ethanol, and C₈H₇N₃ OS were the yield, melting point, color, recovery solvent, molecular formula of z₂, respectively.

2.3.3 Synthesis of Schiff Bases (z_3)

0.579 g, 0.003 mol of z_2 was dissolved in 15 mL of ethanol, then 0.003 mol of different aromatic aldehydes (Salicylaldehyde and 3,4-Dimethoxybenzaldehyde) was added to the mixture with stirring (10 min). Then, 5 drops of Glacial acetic acid (GAA) was added after 5 min of refluxing. Later, the mixture were refluxed for 5–7 h. A precipitated solid was filtered out, dried, and purified using ethanol recrystallization [28]. 77%, 251–253 °C, orange, ethanol, and $C_{15}H_{11}N_3O_2S$ were the yield, melting point, color, recovery solvent, molecular formula of z_3 , respectively.

2.3.4 Synthesis of Mannich Bases (DHOT)

Dissolve 0.003 mol of Schiff bases (z_3) in 15 ml of absolute ethanol, then add formaldehyde (0.003 mol) and then amines (0.003 mol) for each type of amine used gradually to the reaction mixture with continuous stirring in an ice bath for a period of 1 h. That precipitate then left for 24 h at refrigerator, after which a filtration process and recrystallization was performed using absolute ethanol. Used in the preparation (Dicyclohexyl amine) with Schiff bases (z_3) with an equal number of moles. 80%, 192–194 °C, orange, ethanol, and $C_{29}H_{34}N_4O_2S$ were the yield, melting point, color, recovery solvent, molecular formula of DHOT, respectively.

According to the synthesis procedure, the synthesis of intermediates and desired products (DHOT) showed good overall yield with a significant E-factor ($E - factor = \frac{\text{mass of total wastes}}{\text{mass of product}}$) of 2.35, 0.25, 0.29, and 0.25 for z_1 , z_2 , z_3 , and DHOT, respectively. This value is recommended for environmental proposes [29].

2.4 Gravimetric Measurements

Corrosion rates were measured using the conventional method of weight loss. To clean the samples, we followed the steps we described earlier [4–6]. Three hours of exposure in the corrosive solution (1 M HCl) at the specified temperature and inhibitor concentration. Later, the metal samples were cleaned and dried. Corrosion rate was evaluated in the absence and presence of DHOT. Corrosion rates of mild steel were determined over a range of conditions that were specified by experimental design.

2.5 Polarization, Open Circuit, and Impedance Measurements

In electrochemical measurements, a conventional three-electrode (calomel was used as a reference electrode,

platinum wire as a counter electrode, and mild steel as the working electrode) cell (250 ml) was used. The working electrode samples exposed a surface area of 1 cm² to the corrosive solution at the specified conditions. The open circuit potential (OCP) value was evaluated after immersion of the working electrode in the corrosive solution (1 M HCl) for about 120 min. Polarization measurements were conducted in the absence and presence of DHOT under optimum conditions. With respect to OCP, the scan rate is 1.0 mV/s between the cathodic potential range of – 250 mV and the anodic potential range of + 250 mV. A signal amplitude of 10 mV was used for electrochemical impedance spectroscopy (EIS) with a frequency range of 10 kHz to 0.01 Hz. Vertex-One equipment potentiostat (Netherlands) was used for all electrochemical investigations.

2.6 Experimental Design

In order to establish the optimum conditions for a weight loss corrosion rate, a Doehlert experimental design with temperature and DHOT concentration was used. The Doehlert design emphasizes homogeneity in space filling and describes a spherical experimental domain. Despite not being rotatable or orthogonal, this matrix does not dramatically deviate from the necessary characteristics for application. Five Temperature levels (30, 40, 50, 60 and 70 °C) and three DHOT concentrations (0, 75, and 150 ppm) were used. A conversion between real and code variables was carried using the following equations [30]:

$$X_j = \frac{Z_j - Z_j(0)}{\Delta Z_j} \quad (1)$$

where X_j is the coded variable, Z_j is the real variable, $Z_j(0)$ is the center value (50 °C and 75 ppm), and ΔZ_j is the step variation (20 °C and 75 ppm). The coded levels of temperature were calculated as – 1, – 0.866, – 0.5, 0, 0.5, 0.866, and 1, while for DHOT concentration – 0.866, 0, and 0.866. Second order polynomial model (Eq. 2) was suggested to represent corrosion rate as a function of temperature and inhibitor concentration.

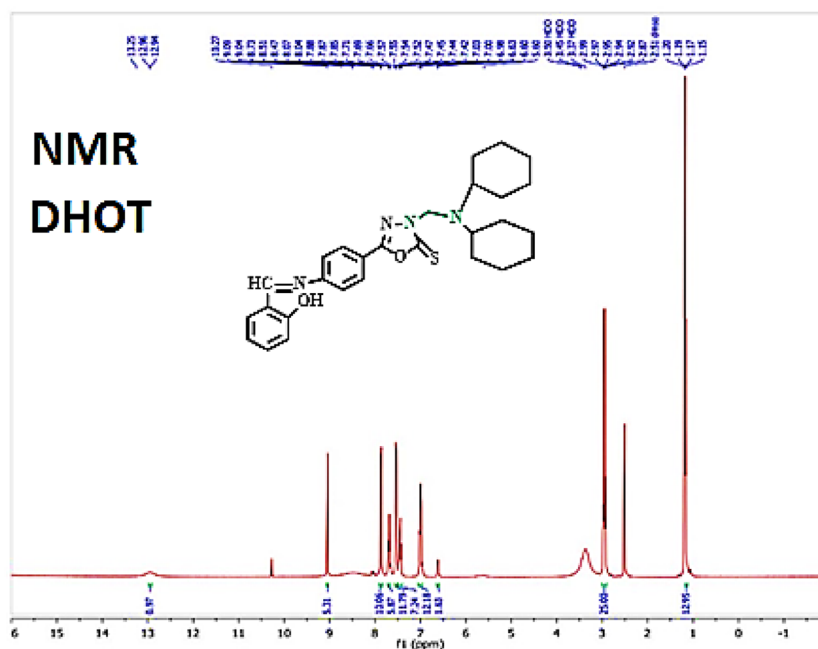
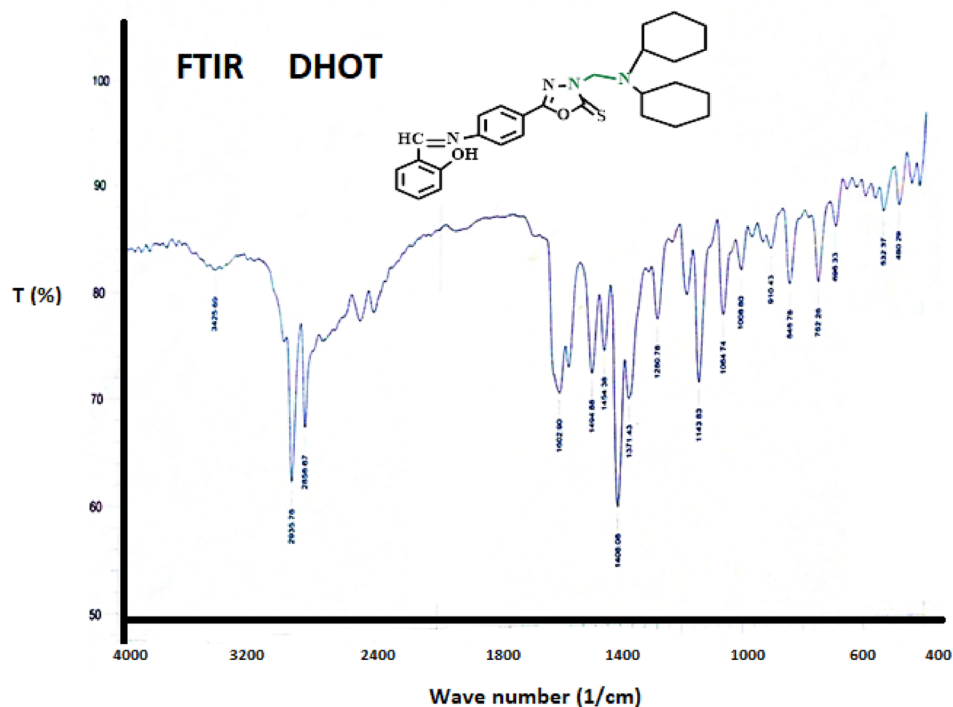
$$Y = h_0 + h_1X_1 + h_2X_2 + h_3X_1^2 + h_4X_2^2 + h_5X_1X_2 \quad (2)$$

Y is the corrosion rate and h_1, h_2, \dots, h_5 are the coefficients of the model.

3 Results and Discussion

3.1 FTIR and ¹H NMR Studies

FTIR and ¹H NMR were illustrated in Fig. 2. The FT-IR spectrum of a compound DHOT shows disappearance

Fig. 2 FTIR and ^1H NMR of DHOT

stretching of NH and appearance band at 3425 cm^{-1} return stretching of OH, and appearance band at 2935.67 cm^{-1} reappearance stretching of CH aliphatic and appearance band a sharp at 1602.90 cm^{-1} return stretching of C=N and appearance band 1494.88 cm^{-1} reappearance stretching of C=C with appearance band (1280 cm^{-1} return stretching of C-N [31]. The ^1H NMR (δ ppm) spectrum of a DHOT $\delta = 9.78\text{ ppm}$ (s, 1H, OH) it corresponds to protons of the

OH and $\delta = 8.72\text{ ppm}$ (s, 1H, $-\text{CH}=\text{N}$) belongs to a proton azomethine, $\delta = 7.02\text{--}7.96\text{ ppm}$ (m, 8H, Ar) returns to the protons of the ring Aromaticity, $\delta = 3.85\text{ ppm}$ (s, 2H, CH_2) returns to the protons of the CH_2 , $\delta = 1.10\text{--}2.02\text{ ppm}$ (m, 22H, cyclohexyl) returns to the protons of the cyclohexyl [31].

3.2 Weight Loss Studies

The method most usually employed to assess corrosion inhibition property is weight loss measurement. It is important for analyzing corrosion rate and corrosion inhibition efficiency due to its easy application and reliability. From weight loss data, corrosion rate can be evaluated according to Eq. 3 [32]:

$$CR = \frac{\Delta W}{A.t} \tag{3}$$

ΔW denotes the weight difference (g), the symbol A denotes the surface area of mild steel sample (m^2), and the symbol t denotes the time of immersion (day). The matrix of Doehlert design and corrosion rate data were collected in Table 1.

The polynomial model of the second-order was generated in term of the real (Eq. 4) and coded (Eq. 5) variables. STATISTICA 10 software was used during regression process that based on of Quasi-Newton and Rosenbrock approximation, with the value of the correlation coefficient (R^2) equal to 0.98 and 0.97 for Eqs. 4 and 5, respectively.

$$P_{C.R.(W.L)} = -664.080 + 30.694T - 1.072C_{DHOT} - 0.094T^2 + 0.046C_{DHOT}^2 - 0.194TC_{DHOT} \tag{4}$$

$$Y = 85.59 + 134.975X_1 - 337.653X_2 - 37.685X_1^2 + 342.825X_2^2 - 335.433X_1X_2 \tag{5}$$

where T is temperature ($^{\circ}C$), C_{DHOT} is the inhibitor concentration of 3-((dicyclohexylamino)methyl)-5-(4-((2-hydroxybenzylidene)amino phenyl)-1,3,4-oxadiazole-2(3H)-thione (ppm), and $P_{C.R.(W.L)}$ is the predicted weight loss corrosion rate in gmd ($g/m^2 \cdot day$). Predicated corrosion rates were close to the experimental one with an average absolute error of 2.7%. Optimization of Eqs. 4 and 5, yields a minimum corrosion rate of 6.6802

gmd at $47.62^{\circ}C$ and 112.1 ppm (-0.126 and 0.431 for coded values of temperature and inhibitor concentration, respectively). However, Fig. 3 shows the statistical results of the model. In Fig. 2A, a comparison between experimental and predicated corrosion rate was illustrated. The effect of model coefficients was observed in Fig. 2B. It is clear that the effect of inhibitor concentration (C and C^2) and interaction of temperature and inhibitor concentration ($T \times C$) was more pronounced than the effect of temperature (T and T^2). While in Fig. 2C and D, the three dimensions surface and contour were illustrated, which show the higher, medium, and lower regions of the corrosion rate as a function of temperature and inhibitor concentration.

3.3 Reaction Kinetics and Adsorption Isotherms

As previously indicated, Eq. 4 can be a useful tool for predicting corrosion rate values as a function of temperatures (30, 40, 50, 60, and $70^{\circ}C$) and DHOT concentrations (0, 25, 50, 75, 100, 125, and 150 ppm). It has an absolute error of 2.17% and a correlation coefficient of 0.98. According to Eq. 4, Fig. 4A illustrates how corrosion rate varies with temperature

and inhibitor concentration. The results sound reasonable, the corrosion rate was increased with temperature and decreased with DHOT concentration increase. Furthermore, as shown in Fig. 4B, inhibition efficiency was increased with inhibitor concentration. However, the inhibition efficiency increased with temperature up to $50^{\circ}C$, a maximum value of 94.08% at 150 ppm DHOT concentration and $50^{\circ}C$, which may be attributed to the chemisorption on inhibitor on metal surface.

Table 1 Experimental Doehlert design for mild steel corrosion in 1 M HCl in presence and absence DHOT

Trial	X_1		X_2		T $^{\circ}C$	C_{DHOT} ppm	Exp. C.R gmd	Predicted C.R gmd	Exp. Error $ \epsilon_i [\%] = \left \frac{P-E}{E} \right $
	Coded		Real						
1	0	0	50	75	85.59	85.59	0.00		
2	1	0	70	75	90.12	182.88	1.02		
3	0.5	0.866	60	150	55.87	36.89	0.33		
4	-0.5	0.866	40	150	25.86	118.62	3.58		
5	-1	0	30	75	5.69	44.07	8.70		
6	-0.5	-0.866	40	Blank	320.19	412.95	0.28		
7	0.5	-0.866	60	Blank	931.17	838.41	0.09		
8	0	0	50	75	85.59	85.59	0.00		
9	0	0	50	75	85.59	85.59	0.00		

The percentage of average absolute error $|\epsilon_i| = 2.17\%$

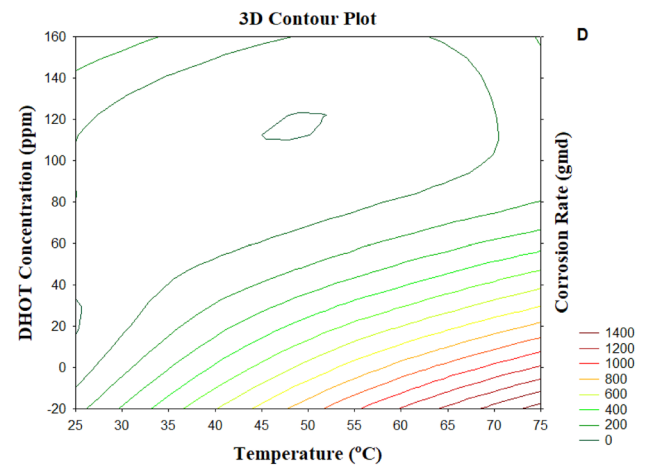
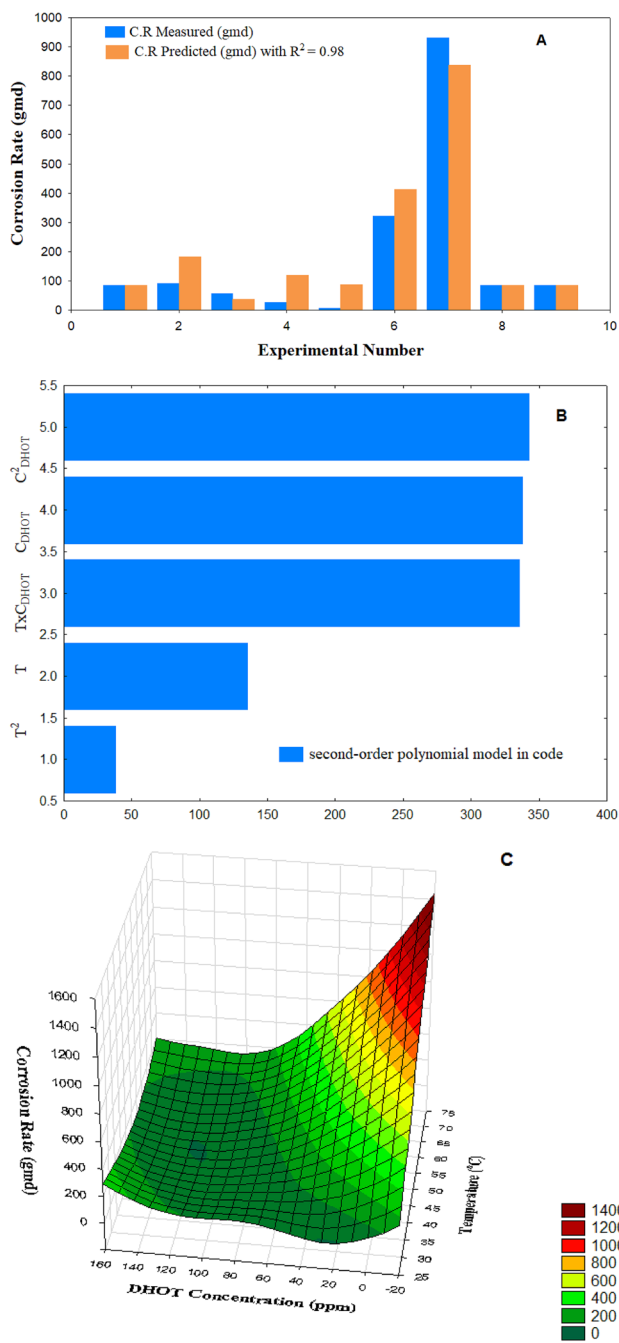


Fig. 3 (continued)

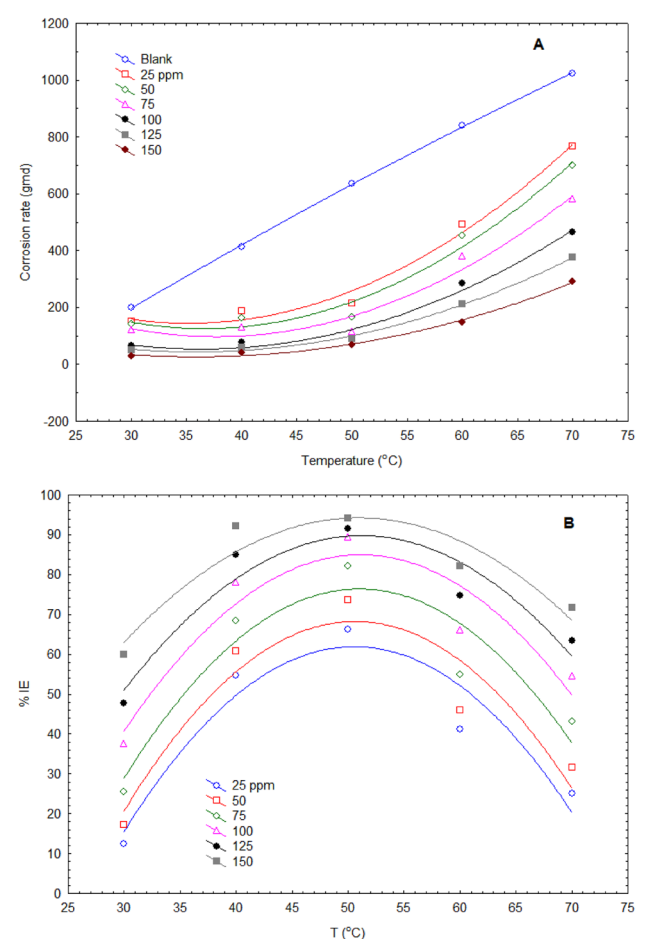


Fig. 4 Variation of corrosion rate with temperature and inhibitor concentration

Fig. 3 Statistical analysis of experimental and predicted corrosion rate. A Experimental corrosion rate versus predicted corrosion rate for DHOT. B Horizontal multiple bar column diagram for DHOT inhibitor. C Surface plot temperature and DHOT concentration versus corrosion rate. D Contour plot temperature and DHOT concentration versus corrosion rate

Further increase of temperature to 60 and 70 °C yields a reduction of inhibitor efficiency. The reason may be due to the desorption of inhibitor molecules at elevated temperature levels. Reaction kinetics and adsorption isotherm represent an

important step in the direction of understanding the inhibition mechanism.

Activation and thermodynamics parameters for the adsorption of DHOT on the steel in are presented in Table 1. These parameters were estimated using the following equations [33]:

$$CR = A \exp\left(-\frac{E_a}{RT}\right) \tag{6}$$

$$CR = \left(\frac{RT}{Nh}\right) \exp\left(\frac{\Delta S_a}{R}\right) \exp\left(-\frac{\Delta H_a}{RT}\right) \tag{7}$$

In Arrhenius equation (Eq. 6) A is frequency factor and E_a is the activation energy, while in transition state equation (Eq. 7), ΔH_a (enthalpy of activation), ΔS_a (entropy of activation), constant of Plank's is h, and Avogadro's number is N. These equations were linearized and illustrated in Fig. 5. The slopes and intercepts were used to determine the data of Table 2. As is readily observed, enthalpy and activation energy both fluctuate similarly. The difference between the

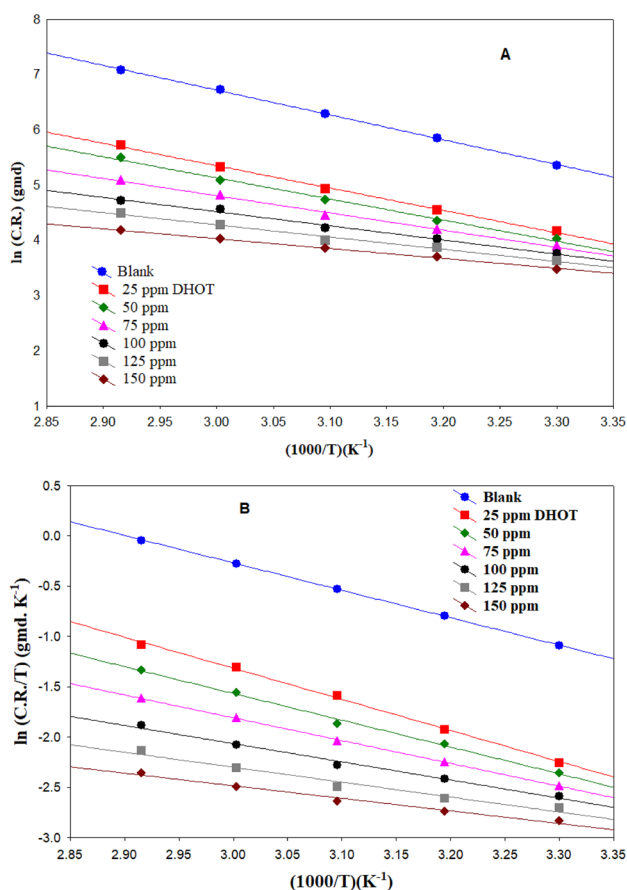


Fig. 5 Activation representation of corrosion rate of mild-carbon steel in DHOT-1 M HCl **A** Arrhenius plots **B** transition state plots

Table 2 Mild-steel corrosion kinetic parameters at different concentrations of DHOT

C_{DHOT} (ppm)	A (gmd)	E_{act} (J/mol)	ΔH_{act} (J/mol)	ΔS_{act} (J/mol. K)
Blank	1.6×10^3	37.290	22.657	-196.44
25	3.8×10^2	33.592	25.705	-204.68
50	2.9×10^2	31.753	22.137	-207.37
75	1.9×10^2	25.865	18.860	-209.81
100	1.3×10^2	21.325	15.031	-212.55
125	9.9×10^1	18.386	12.354	-214.92
150	7.3×10^1	14.837	10.393	-216.73

activation energy and enthalpy in the acidic solution with and without the inhibitor seems unreasonable. This might be due to the fact that inhibitor molecules cover more metal surfaces at higher temperatures, or it might be because the formation of the chemisorbed layer occurs more quickly than its dissolution [34]. The positive enthalpy values reflect the endothermic nature of the steel dissolution process. The values of A (frequency factor) in the presence of DHOT were lower than the blank acidic solution, which is beneficial for the steel corrosion process. The activated complex suggests an association step rather than a dissociation phase during the transition from reactant to activated complex due to the large negative value of ΔS_a in the DHOT-acid solution [35].

For more information on the mode and type of adsorption of DHOT on the steel surface, the experimental data with Langmuir adsorption isotherms (Eq. 8) was tested. Indeed, the installation of isotherms that better describe the adsorption behavior of corrosion inhibition process [36].

$$\frac{C}{\theta} = \frac{1}{K} + C \tag{8}$$

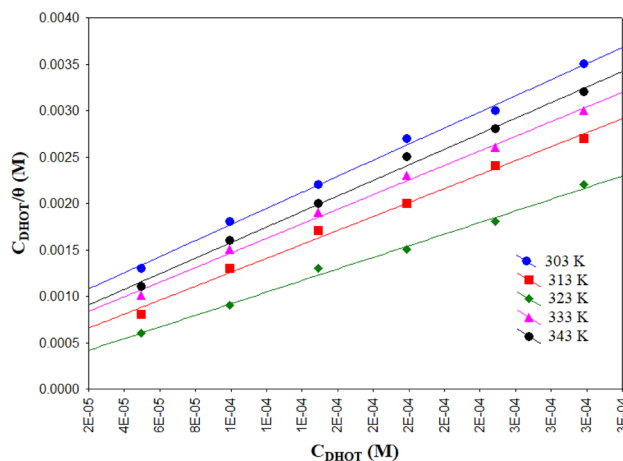


Fig. 6 Langmuir adsorption isotherm on mild steel surface in 1 M HCl solution at different DHOT concentrations

Table 3 Thermodynamic parameters for the DHOT adsorption

T (K)	Slope	K _{ads} (l/mol)	ΔG _{ads} (kJ/mol)	R ²	ΔS _{ads} (kJ/mol. K)	ΔH _{ads} (kJ/mol)	R ²
303	1.062	909.1	- 27.2794	0.9966	0.155	19.8855	0.976
313	1.029	1111	- 28.7016	0.9932			
323	1.002	1250	- 29.9352	0.9935			
333	1.010	1428	- 31.2305	0.9949			
343	1.053	2500	- 33.7654	0.9951			
Average value	1.031	1439.6	- 30.1824	0.9947			

C is the inhibitor concentration, K is adsorption constant, and θ is the surface coverage. Equation 8 was plotted in Fig. 6. The results were collected in Table 3. The high linearity and fitting of the data confirmed the obeying of the Langmuir adsorption isotherm. This also obvious from the slope and correlation coefficients that both close to unity (Table 2).

K values can be used to gauge the strength of the adsorption forces between inhibitory molecules and the metal surface [37]. Using Eq. 9, the K is related to the standard free energy of adsorption (ΔG_{ads}) [38]:

$$K = -\frac{1}{55.5} \exp\left(-\frac{\Delta G_{ads}}{RT}\right) \tag{9}$$

55.55 is the concentration of water in the solution in molarity (M), R is the universal gas constant, and T is the temperature (K). An average value of ΔG_{ads} was - 30.1824 kJ/mol. The negative values indicate the stability and spontaneous adsorption process. Furthermore, a chemical adsorption was suggested since the ΔG_{ads} values were found to be higher than - 20 kJ/mol [28]. Van't Hoff equation (Eq. 10) and Eq. 11 were used to estimate the values of adsorption enthalpy (ΔH_{ads}) and adsorption entropy (ΔS_{ads}) [39]. Both equation are illustrated in Fig. 7.

$$\ln K = -\frac{\Delta H_{ads}}{RT} + const \tag{10}$$

$$\Delta G_{ads} = \Delta H_{ads} - T\Delta S_{ads} \tag{11}$$

Table 3 shows that these findings appear to conflict with commonly held beliefs about adsorption phenomena. It is widely assumed that adsorption is exothermic. The negative sign for adsorption heat and a decrease in adsorption entropy were recommended [40]. Organic molecules adsorption in aqueous media results in water molecule desorption. Adsorption of organic molecules at the metal-solution interface is a replacement process, with each DHOT molecule repelling a water molecule. Adsorption of DHOT molecules and desorption of water molecules resulted in a total of ΔS_{ads}. As a result, a rise in solvent entropy can be linked to an increase in entropy [41].

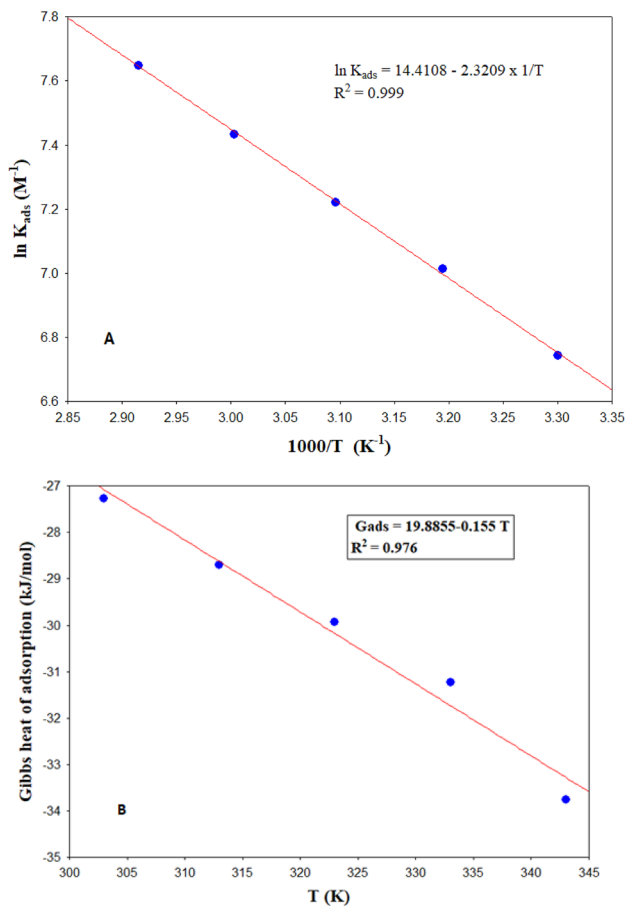


Fig. 7 A Adsorption constant against temperature B standard adsorption free energy against temperature for DHOT adsorption on low-carbon steel

3.4 Electrochemical Investigations

To confirm the outcomes of gravimetric analyses, an electrochemical measurements were conducted. An open circuit potential (OCP) and potentiodynamic polarization (PDP) were evaluated at optimum conditions as shown in Fig. 8. In Fig. 8A, the OCP of inhibitor moved in positive direction as compared with the absence of DHOT that signifying the deviation toward the noble region. However, the OCP

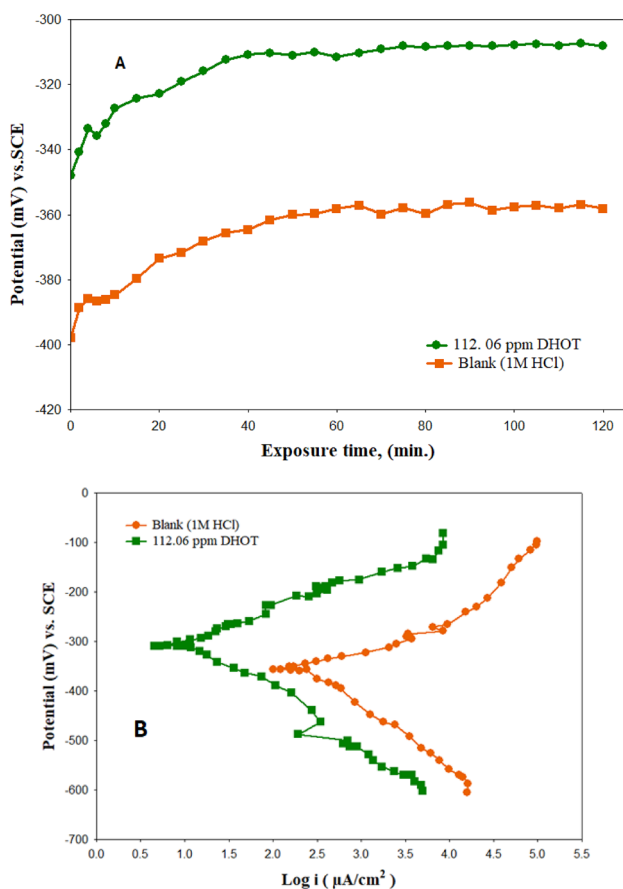


Fig. 8 Electrochemical illustrations for corrosion of mild-carbon steel in 1 M HCl solution with and without DHOT at optimum conditions **A** Open Circuit Potential (OCP) **B** Tafel polarization

shifting was within the range of ± 85 mV, which suggests the mixed-type DHOT behavior [42].

The effect of DHOT on cathodic and anodic reactions was investigated using PDP after 3 h immersion in HCl without and with DHOT at optimum conditions (Fig. 8B). Corrosion current density (i_{corr}), corrosion potential (E_{corr}), resistance polarization (R_p), and slope of anodic and cathodic branches (β_a and β_c), are listed in Table 4. In addition, the corrosion inhibition efficiency was calculated using Eq. 10 [43].

$$\% IE_{PDP} = \frac{i_{corr}^o - i_{corr}}{i_{corr}^o} \times 100 \tag{12}$$

In this equation, i_{corr}^o and i_{corr} are the corrosion current density in the absence and presence of optimum concentration of DHOT, respectively. According to Fig. 8B, it can be realized that in the presence of DHOT, the current density has decreased in both anodic and cathodic branches compared to the blank.

Again, the value of E_{corr} shift was lower than ± 85 mV in presence of DHOT, it was found that the shift was 47.07 mV towards anodic branch, so DHOT acted as a mixed-type inhibitor with more effect on anodic process. Inhibitor efficiency was 98.86% at optimum conditions. The reduction of the corrosion current density in the presence of DHOT indicates the formation of protective layer on the metal surface.

Further electrochemical studies are conducted. The corrosion behavior of mild steel in 1 M HCl in the absence and in the presence of DHOT was studied by the electrochemical impedance spectroscopy (EIS) technique at optimum conditions. Equivalent circuit, Nyquist diagrams, and Bode diagrams are shown in Fig. 9. Furthermore, inhibition efficiency according to EIS calculations can be calculated using Eq. 13 [43].

$$\% IE_{EIS} = \frac{R_{ct} - R_{ct}^o}{R_{ct}} \times 100 \tag{13}$$

R_{ct} and R_{ct}^o are the charge transfer resistance in the absence and presence, respectively. All characteristic and kinetics parameters associated to the impedance investigations such as, solution resistance (R_s), charge transfer resistance (R_{ct}), double-layer capacitance (C_{dl}), and ($\%IE_{EIS}$) are given in Table 5. The Nyquist graph illustrates that the diameter of the capacitive loop increases with the addition of the inhibitor, affirming the initiation of a protective barrier on the metal surface [44]. The increased of modulus and phase angle values of inhibited Bode plots indicate that surfaces become smoother due to adsorption of DHOT molecules on the steel surface.

Mathematically, C_{dl} can be given by Eq. 14 [45].

$$C_{dl} = \frac{\epsilon_o \epsilon A}{d} \tag{14}$$

In above equation, ϵ_o designates to the permittivity, ϵ specifies dielectric constant of protective layer, d is thickness of protective layer, and A is the electrode surface area. It is

Table 4 Polarization parameters for mild steel in 1 M HCl at optimum conditions

Condition	β_a (mV)	β_c (mV)	I_{corr} ($\mu A/cm^2$)	R_p ($\Omega.cm^2$)	E_{corr} (mV) SCE	OCP (mV) SCE	IE_{PDP}
Blank	83	- 111	2337.66	8.82	- 356.06	- 358.13	98.86%
DHOT	89	- 120	26.72	830.41	- 308.99	- 308.17	

Fig. 9 Equivalent circuit, Nyquist diagrams, and Bode diagrams of mild steel in 1 M HCl in the absence and presence of optimum DHOT concentration

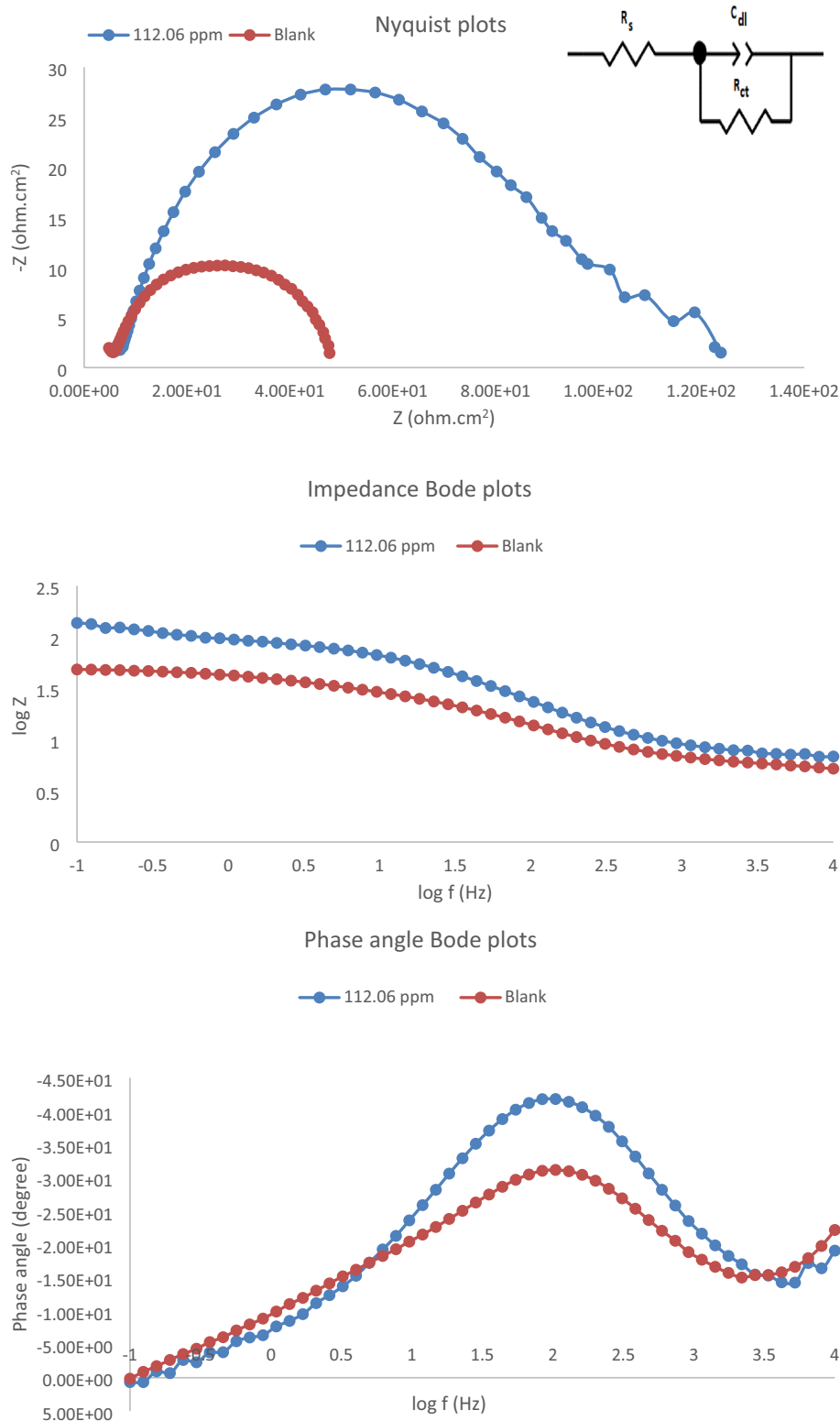


Table 5 EIS parameters for mild steel in 1 M HCl at optimum conditions

Condition	R_s ($\Omega \cdot \text{cm}^2$)	R_{ct} ($\Omega \cdot \text{cm}^2$)	C_{dl} (F)	IE_{EIS}
Blank	5.721	05.84	1.06×10^{-4}	91.01%
DHOT	7.429	64.91	6.81×10^{-5}	

clear that the addition of optimum concentration of DHOT provided lower C_{dl} value. This perhaps attributed to the water molecules replacement by DHOT inhibitor molecules at the metal surface. Moreover, C_{dl} values decrease with addition of DHOT. It indicates that the inhibitor molecules functioned by adsorption on the metal surface because of a decrease in the local dielectric constant and/or an increase in the thickness of the electrical double layer [46].

3.5 Surface Morphology Investigations

The surface morphology of low-carbon steel after 3 h immersion in 1 M HCl was investigated in the absence

and presence of DHOT at optimum conditions. As shown in SEM images (Fig. 10A, B, and C, upper images), the steel surface before immersion (Fig. 10A) looks smooth and undamaged. The damaged was illustrated after immersion in the corrosive acidic solution (Fig. 10B). However, adding the optimum concentration of DHOT to the acidic solution prevented the formation of corrosion products and a relatively uniform and smooth surface can be seen (Fig. 10B). Similar behavior was observed via Optical Microscope Tomography (OMT) images (Fig. 10A, B, and C, lower images).

AFM analysis was conducted (Fig. 11) to demonstrate the effect of DHOT on the roughness and microstructure of the low-carbon steel surface. The average roughness (R_a) of the mild-steel samples before immersion, blank acidic solution, and inhibited acidic solutions were 55.07, 162.4, and 137.7 nm, respectively. The decline in the roughness in the presence of inhibitor may be attributed to metal corrosion reduction.

XRD was recorded to investigate the composition of the steel before immersion in acidic solution, after immersion in an acidic solution without DHOT, and in the presence of DHOT at optimum conditions. As shown in Fig. 12 the

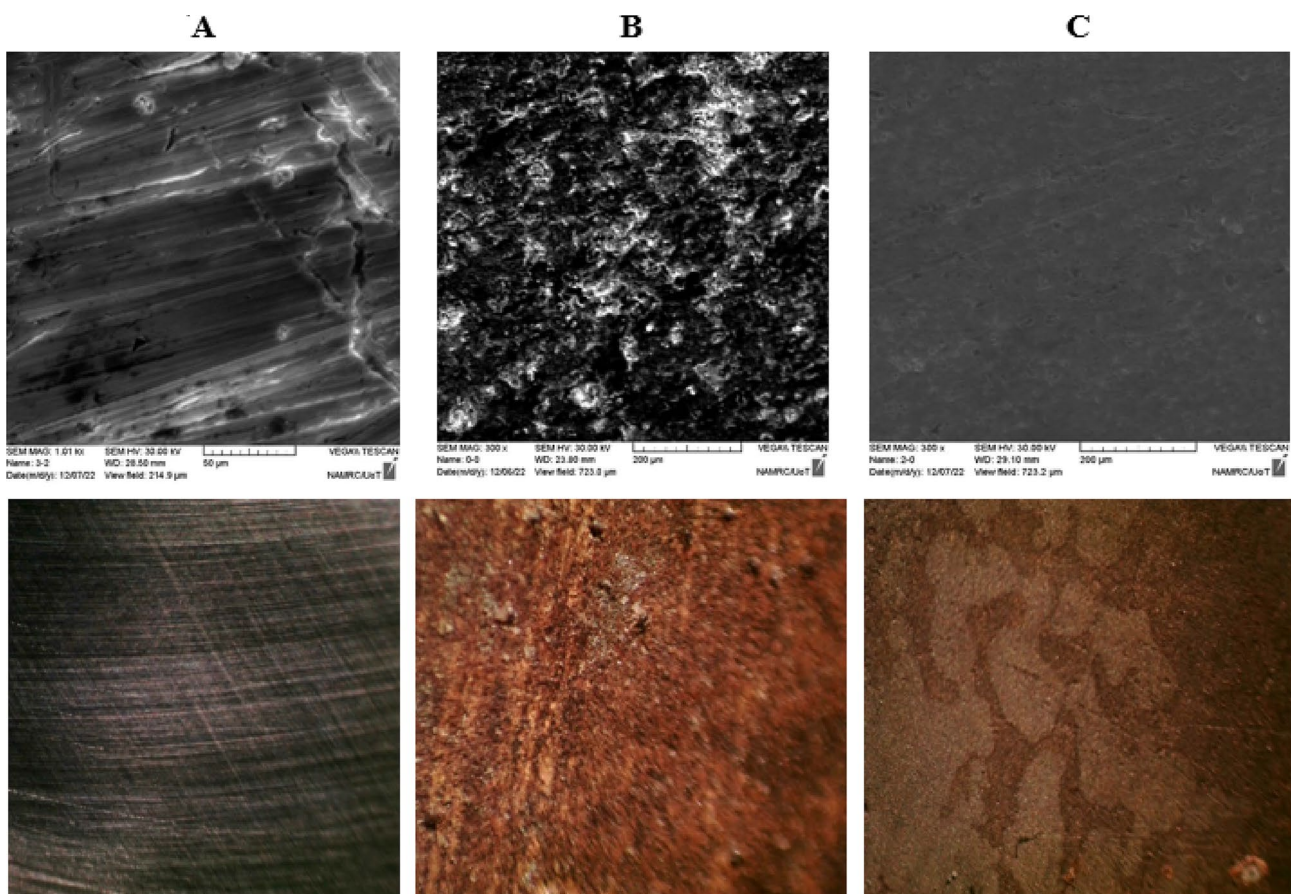


Fig. 10 The SEM and OMT (magnification power 100 ×) images for mild steel **A** polished sample before corrosion test **B** sample immersed in 1 M HCl in absence and presence **C** of DHOT at optimum conditions

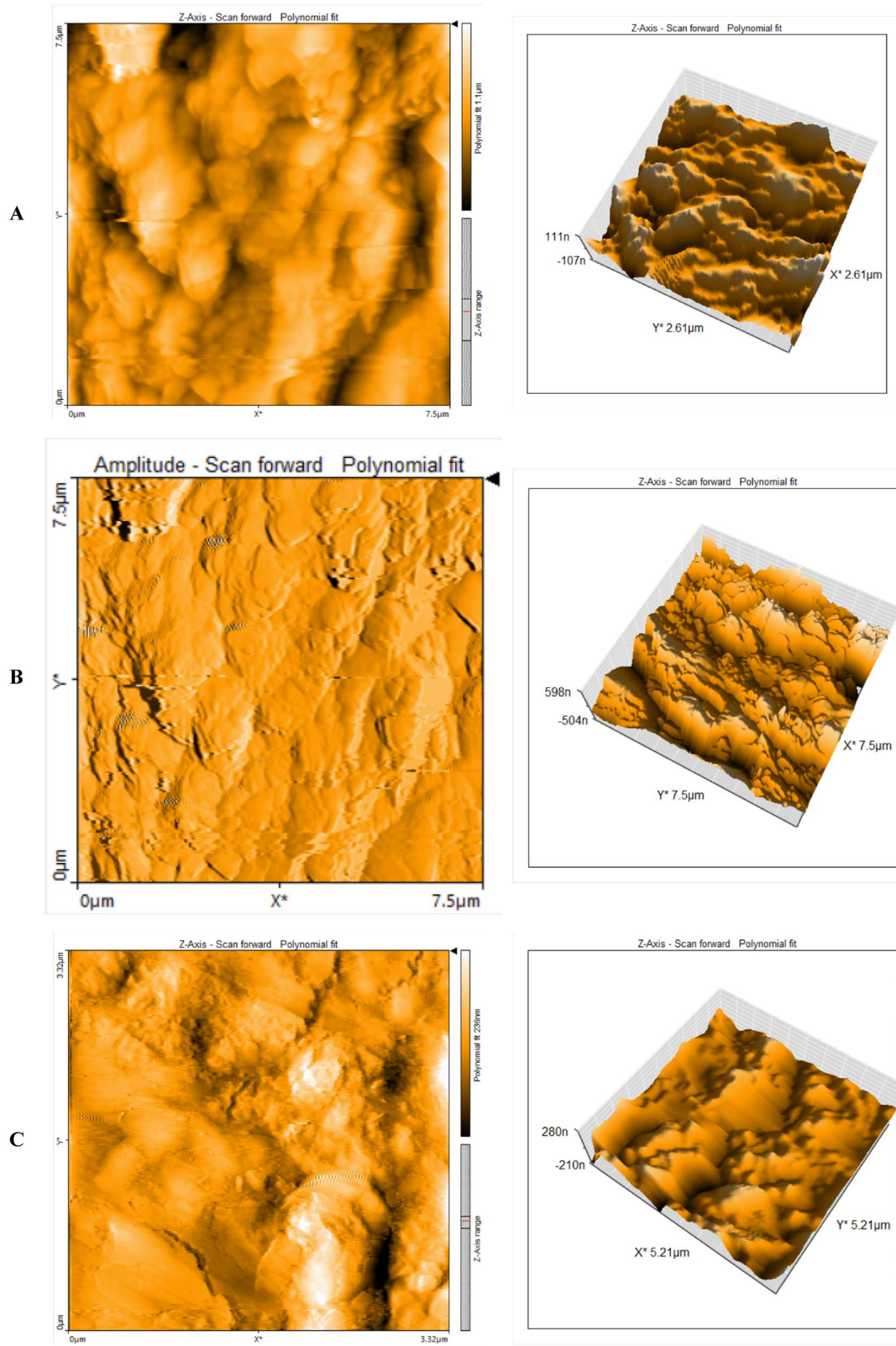


Fig. 11 AFM surface images, with corresponding roughness parameters, after 3 h corrosion of mild steel in 1 M HCl solution at optimum conditions **A** polished sample before corrosion test **B** without inhibitor, and **C** in the presence of DHOT

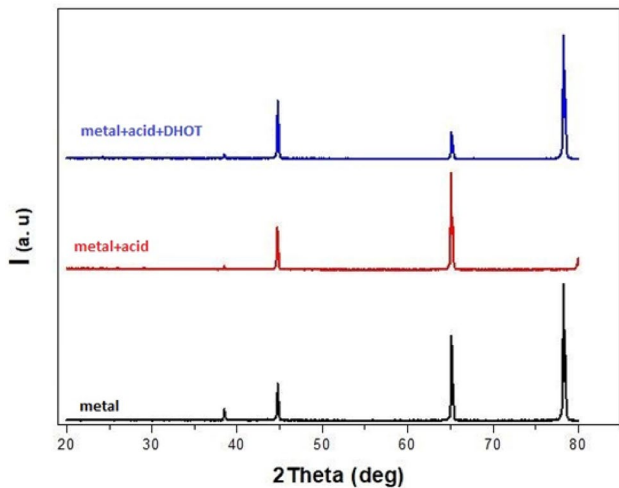


Fig. 12 XRD surface images after 3 h corrosion of mild steel in 1 M HCl solution at optimum conditions for polished sample before corrosion test, without inhibitor, and in the presence of DHOT

peaks at 2θ around 36° are attributed to $\text{Fe}_2\text{O}_3/\text{FeCl}_3$ which are due to the presence of corrosion product on the blank steel surface. Also, peaks at $2\theta = 45^\circ$, and 65° are related to Fe [47]. Comparing the XRD patterns shows that the corrosion product peaks disappeared after adding DHOT. Furthermore, the intensification of the peak at 45° and the appearance of a peak at 65° (peaks related to Fe metal) can confirm the assumption of the interaction between DHOT and steel surface, which corroborate the production of fewer corrosion products.

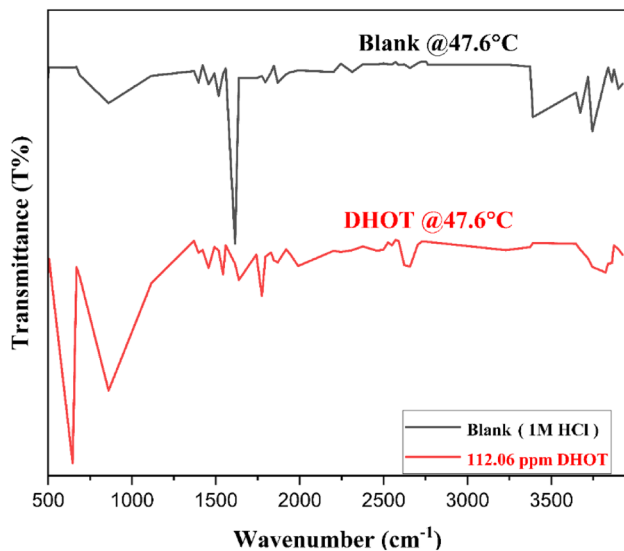


Fig. 13 FT-IR spectrum of sample corrosion products for blank, with DHOT in 1 M HCl at optimum conditions

3.6 FTIR Investigations

FTIR spectra mild steel surface corrosion products immersed in acidic solution in the absence and presence of DHOT were recorded at optimum conditions. In the presence of inhibitor, which can be seen in Fig. 13, the appearance of peaks between 1500 and 2000 are related to C=C stretching of the aromatic ring and C=O stretching are observed at 1605 cm^{-1} and 1715 cm^{-1} , respectively [48, 49]. The peaks between 1200 and 1500 cm^{-1} are correlated to $-\text{H}$ bending. The peaks between 400 cm^{-1} and 1000 cm^{-1} can be due to the aliphatic and aromatic C-H bending. In the absence of the DHOT, some similar peaks were observed in the corrosion products. This outcome reveals the adsorption of DHOT molecules. Additionally, shifting the peaks in the region of $1700\text{--}1750\text{ cm}^{-1}$ and from 1600 to 1630 cm^{-1} can of C=O stretching and C=C stretching, respectively, may be attributed to the development of a complex between DHOT and iron ions [47, 50]. In brief, results showed that functional groups, aromatic rings, nitrogen-containing, and oxygen-containing groups in the DHOT structure could cause the interaction between inhibitor molecules and the metal surface.

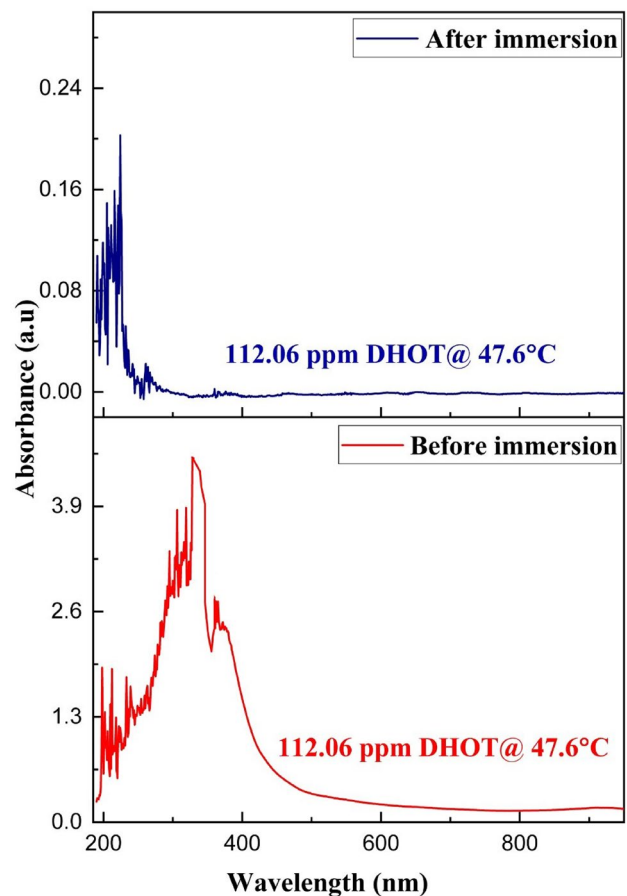


Fig. 14 UV-Vis spectra of 1 M HCl solution containing optimum concentration of DHOT before and after immersion

3.7 UV-Vis Investigations

The probability of complex formation between the DHOT molecule and iron ions was considered using the UV-Vis investigation. Figure 14 shows the UV-Vis spectrum before and after mild steel immersion in the acidic solution containing DHOT at optimum conditions. The UV-Vis spectrum of the solution before immersion, included several peaks. The maximum peak was centered at 340 nm, which may be attributed to O-H bonds. Others peaks in the range of 200–300 nm can be attributed to $\pi-\pi^*$ transitions of C=C bonds in aromatic rings and C=O bonds [51, 52]. After 3 h of mild steel immersion in the corrosive solution containing the DHOT, the intensity of the absorption peaks related to $\pi-\pi^*$ and $n-\pi^*$ transitions were decreased. In addition, the UV-Vis spectrum was shifted to a lower wavelength value. These observations may correspond to the adsorption of DHOT molecules on the metal surface and the formation of an organic-inorganic complex by the interaction between pair electrons of DHOT molecule and vacant orbital of $\text{Fe}^{2+}/\text{Fe}^{3+}$ [51, 52].

3.8 Quantum Chemical and Theoretical Investigations

Computational methods are understood to have potential applications. In the subject of corrosion, it is peculiarly employed in the design and research of organic corrosion inhibitors [53, 54]. The ArgusLab 4.0.1 software (Thompson and Planaria Software LLC) was used to do quantum chemistry simulations to look into the charge distribution of the DHOT molecule. The optimization of molecule surface and energies was estimated using the PM3-SCF method with a maximum number of 200 iterations and 10^{-10} kcal/mol of energy convergence. Mulliken distributions, mapped-density surface, HOMO, and LUMO were calculated. It was presented in Figs. 15 and 16, respectively. It has been determined that the easier an atom

is drawn to a metal surface, the more negative the adsorbed center's atomic partial charges are. It is clear that the negative charges are concentrated on S, O, N, and some C atoms. Table 6 shows quantum chemical parameters that calculated. These are mainly the highest occupied (E_{HOMO}), lowest unoccupied (E_{LUMO}), energy gap (E_{gap}), heat of formation (ΔH_f), fraction of electron transfer (ΔN), and dipole moment (μ). The tendency of the inhibitor to give electrons to the metal's vacant d orbital increases with the inhibitor's HOMO energy, leading to a higher corrosion inhibition efficiency. Furthermore, as the gap between HOMO-LUMO energies reduces and inhibitor efficiency improves, the lower the LUMO energy, the easier the acceptance of electrons from the metal surface.

The number of transferred electrons (ΔN) was also calculated as in the following equation [55]:

$$\Delta N = \frac{X_{\text{Fe}} - X_{\text{DHOT}}}{2(\eta_{\text{Fe}} + \eta_{\text{DHOT}})} \quad (15)$$

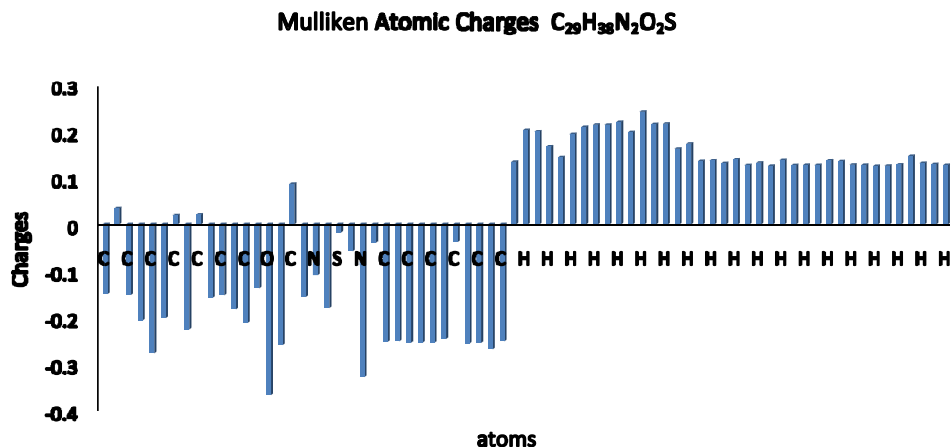
Electronegativity of DHOT and steel were denoted as X_{DHOT} and X_{Fe} (equal 7 eV/mol in case of Fe), respectively. η_{Fe} (equal zero eV/mol in case of Fe) and η_{DHOT} stand for the hardness of steel and DHOT, respectively. Electronegativity and hardness were related to electron affinity (A) and ionization potential (I) according to Eq. 16 and 17 [56, 57].

$$x = \frac{I + A}{2} = \frac{-(E_{\text{HOMO}} + E_{\text{LUMO}})}{2} \quad (16)$$

$$\eta = \frac{I - A}{2} = \frac{-(E_{\text{HOMO}} - E_{\text{LUMO}})}{2} \quad (17)$$

ΔN demonstrated an inhibition effect caused by electron donation. According to Lukovits's investigation [58, 59], if ΔN is lower than 3.6, the inhibition efficiency increased as the metal surface's electron-donating ability increased. In current work, hence the fraction of electron transfer was

Fig. 15 Mulliken atomic charges distribution of DHOT molecule



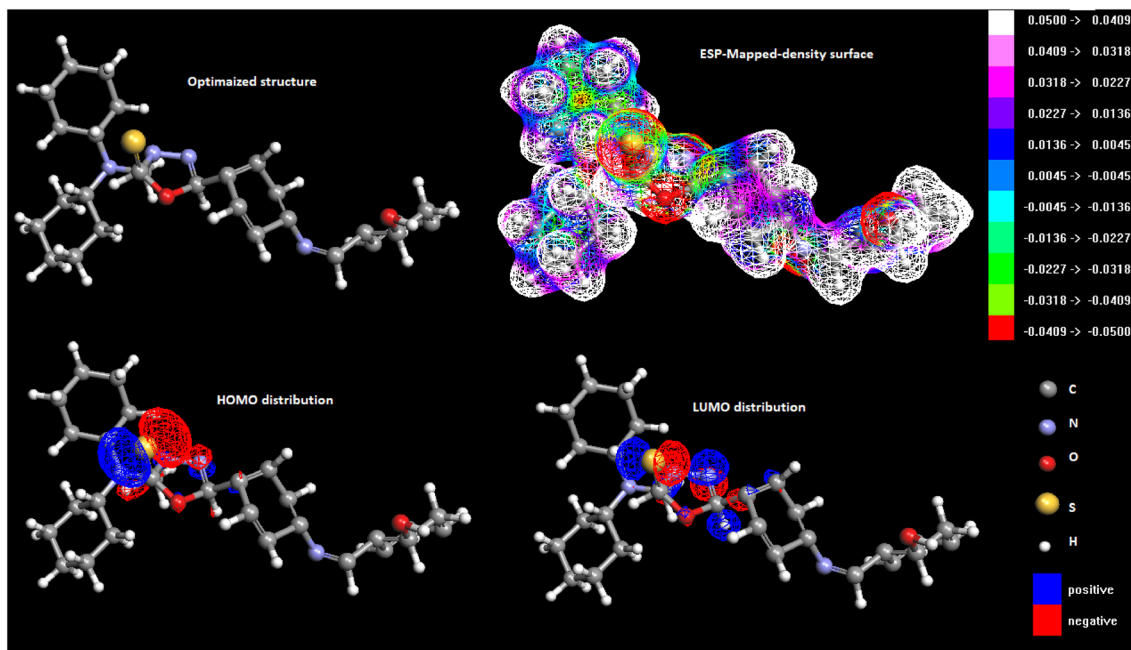


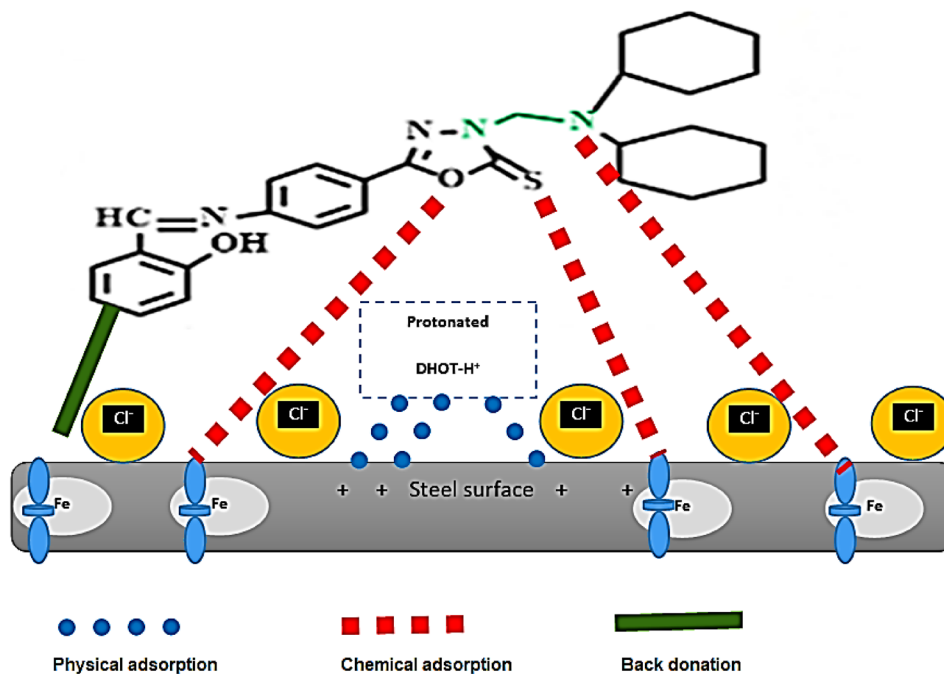
Fig. 16 Optimized DHOT structure, mapped-density surface, HOMO, and LUMO distribution

Table 6 Quantum chemical parameters of DHOT

E_{HOMO} (eV)	E_{LUMO} (eV)	E_{gap} (eV)	ΔN	ΔH_f (kcal/mol)	μ (dybe)
- 7.919	- 0.778	7.141	0.371	151.81	5.647

0.371 (DHOT is electron donor and mild steel is the acceptor). DHOT is linked to the surface, forming a corrosion-inhibiting adsorption layer.

Fig. 17 Mechanism of inhibition DHOT on mild steel surface



3.9 Mechanism of Inhibition

The bonding characteristic between inhibitor molecules and metal atoms determines the adsorption behavior of inhibitor molecules [60]. The proposed schematic for the adsorption of DHOT on the surface of mild steel is shown in Fig. 17. The configuration was developed using theoretical and experimental considerations. The mild steel surface is positively charged in hydrochloric acid [61, 62]. Moreover, organic molecules can protonate in acidic conditions, which can facilitate electrostatic physical interactions with a charged metal surface with chloride ions acting as intermediaries to their cationic versions [63]. In other words, the deposited chloride ions have an electrostatic effect on the positively charged inhibitory compounds. The first connection between the inhibitor and the metal surface is now physical adsorption. Second, following the release of H₂ in the cathodic process, the protonated inhibitor molecules revert to their neutral state and are chemisorbed onto the metal surface via donor interactions between the free electron pairs of N, S, and O heteroatoms and the vacant d orbital of the iron atoms [64]. Back-donation interactions are created as a result of the excessive accumulation of negative charge caused by this type of electron transfer on the metal surface.

4 Conclusion

According to experimental and theoretical studies, the synthesized DHOT has a substantial inhibitory efficiency in a 1 M HCl solution. DHOT's corrosion inhibition efficacy increased with concentration, showing inhibitor adsorption on the mild-steel surface. The Tafel polarization data support the inhibitor's mixed-type nature. Thermodynamic and adsorption investigations revealed that DHOT adsorbed on metal surfaces. The adsorption was according to the Langmuir adsorption isotherm. SEM, AFM, and optical measurements confirmed the gravimetric and electrochemical calculations. Their images indicated the creation of an inhibitor protective layer on the metal surface. The DHOT experimental results agreed with the theoretical calculations derived by quantum chemistry. In brief, the synthesis of corrosion inhibitor provides advantages such as high inhibition efficiency, low inhibitor concentration, short working period, and strong bonding between the molecules of the inhibitor and the surface of mild steel. It can be a promising corrosion control method for developing new protective materials.

Author Contributions ZIJ: data collection. KHR: conceptualization and methodology, and software. KFAL-A: synthesis of corrosion inhibitor and diagnosis, AAK: supervision, analysis, software, discussion, writing, reviewing, and editing.

Funding The authors have not disclosed any funding.

Data Availability All data are available in the research.

Declarations

Conflict of interest The authors declare no competing interests.

Ethical Approval Not applicable.

References

- Berrissoul A, Ouarhach A, Benhiba F, Romane A, Zarrouk A, Guenbour A et al (2020) Evaluation of *Lavandula mairei* extract as green inhibitor for mild steel corrosion in 1 M HCl solution. Experimental and theoretical approach. J Mol Liq 313:113493. <https://doi.org/10.1016/j.molliq.2020.113493>
- Rashid KH, Khadom AA (2020) 3-Methoxypropyl-amine as corrosion inhibitor for X80 steel in simulated saline water. J Mol Liq 319:114326. <https://doi.org/10.1016/j.molliq.2020.114326>
- Khadom A, Rashid K (2018) Adsorption and kinetics behavior of kiwi juice as a friendly corrosion inhibitor of steel in acidic media. World J Eng 15(3):388–401. <https://doi.org/10.1108/WJE-08-2017-0246>
- Fadhil AA, Khadom AA, Ahmed SK, Liu H, Fu C, Mahood HB (2020) Portulaca grandiflora as new green corrosion inhibitor for mild steel protection in hydrochloric acid: quantitative, electrochemical, surface and spectroscopic investigations. Surf Interfaces 20:100595. <https://doi.org/10.1016/j.surfin.2020.100595>
- Khadom AA (2015) Kinetics and synergistic effect of iodide ion and naphthylamine for the inhibition of corrosion reaction of mild steel in hydrochloric acid. React Kinet Mech Catal 115(2):463–481. <https://doi.org/10.1007/s11144-015-0873-9>
- Khadom AA, Yaro AS (2011) Modeling of corrosion inhibition of copper-nickel alloy in hydrochloric acid by benzotriazole. Russ J Phys Chem A 85(11):2005–2012. <https://doi.org/10.1134/S0036024411110148>
- Shahini MH, Ramezanzadeh M, Bahlakeh G, Ramezanzadeh B (2021) Superior inhibition action of the Mish Gush (MG) leaves extract toward mild steel corrosion in HCl solution: theoretical and electrochemical studies. J Mol Liq 332:115876. <https://doi.org/10.1016/j.molliq.2021.115876>
- Swathi NP, Samshuddin S, Aljohani TA, Rasheeda K, Alva VD, Alomari FY, Alamri AH (2022) A new 1, 2, 4-triazole derivative as an excellent corrosion inhibitor: electrochemical experiments with theoretical validation. Mater Chem Phys 291:126677. <https://doi.org/10.1016/j.matchemphys.2022.126677>
- Fouda AEAS, Etaiw SEH, Ismail MA, Abd El-Aziz DM, Eladl MM (2022) Novel naphthylbithiophene derivatives as corrosion inhibitors for carbon steel in 1 M HCl: electrochemical, surface characterization and computational approaches. J Mol Liq 367:120394. <https://doi.org/10.1016/j.molliq.2022.120394>
- Al-Uqaily RA, Al-Bayat SA, Khadom AA, Kadhim MM (2022) Inhibitive performance of 4-Methoxyphenethylamine on low-carbon steel in 1 M hydrochloric acid: kinetics, theoretical, and mathematical views. J Mol Liq 350:118523. <https://doi.org/10.1016/j.molliq.2022.118523>

11. Carlos MF, Barboza GK, Echevarria A (2022) Anticorrosive effect of halogenated aniline enaminoesters on carbon steel in HCl. *Int J Corros*. <https://doi.org/10.1155/2022/7218063>
12. Khadom AA, Yaro AS (2011) Protection of low carbon steel in phosphoric acid by potassium iodide. *Prot Met Phys Chem Surf* 47:662–669. <https://doi.org/10.1134/S2070205111050078>
13. Elabbasy HM, Gadow HS (2021) Study the effect of expired tenoxicam on the inhibition of carbon steel corrosion in a solution of hydrochloric acid. *J Mol Liq* 321:114918. <https://doi.org/10.1016/j.molliq.2020.114918>
14. Selatnia I, Sid A, Benahmed M, Ozturk T, Gherraf N (2018) Synthesis and characterization of a bis-pyrazoline derivative as corrosion inhibitor for A283 carbon steel in 1M HCl: electrochemical, surface, DFT and MD simulation studies. *Prot Met Phys Chem Surf* 54(6):1182–1193. <https://doi.org/10.1134/S2070205118060229>
15. Sehmi A, Ouici HB, Guendouzi A, Ferhat M, Benali O, Boudjellal F (2020) Corrosion inhibition of mild steel by newly synthesized pyrazole carboxamide derivatives in HCl acid medium: experimental and theoretical studies. *J Electrochem Soc* 167(15):155508. <https://doi.org/10.1149/1945-7111/abab25>
16. Mrani SA, El Arrouji S, Karrouchi K, El Hajjaji F, Alaoui KI, Rais Z, Taleb M (2018) Inhibitory performance of some pyrazole derivatives against corrosion of mild steel in 1.0 M HCl: electrochemical, MEB and theoretical studies. *Int J Corros Scale Inhib* 7(4):542–569. <https://doi.org/10.17675/2305-6894-2018-7-4-5>
17. Laadam G, Benhiba F, El Faydy M, Titi A, Al-Gorair AS, Alsharreef M et al (2022) Anti-corrosion performance of novel pyrazole derivative for carbon steel corrosion in 1 M HCl: Computational and experimental studies. *Inorg Chem Commun* 145:109963. <https://doi.org/10.1016/j.inoche.2022.109963>
18. Grudic V, Boskovic I, Radonjic D, Jacimovic Z, Knezevic B (2019) The electrochemical behavior of Al alloys in NaCl solution in the presence of pyrazole derivative. *Iran J Chem Chem Eng (IJCCCE)* 38(2):127–138. <https://doi.org/10.30492/IJCCCE.2019.30659>
19. Singh A, Ansari KR, Chauhan DS, Quraishi MA, Lgaz H, Chung IM (2020) Comprehensive investigation of steel corrosion inhibition at macro/micro level by ecofriendly green corrosion inhibitor in 15% HCl medium. *J Colloid Interface Sci* 560:225–236. <https://doi.org/10.1016/j.jcis.2019.10.040>
20. Ahmed SK, Ali WB, Khadom AA (2019) Synthesis and characterization of new triazole derivatives as corrosion inhibitors of carbon steel in acidic medium. *J Bio Tribo Corros* 5(1):15. <https://doi.org/10.1007/s40735-018-0209-1>
21. Abdulridha AA, Allah MAAH, Makki SQ, Sert Y, Salman HE, Balakit AA (2020) Corrosion inhibition of carbon steel in 1 M H₂SO₄ using new Azo Schiff compound: electrochemical, gravimetric, adsorption, surface and DFT studies. *J Mol Liq* 315:113690. <https://doi.org/10.1016/j.molliq.2020.113690>
22. El Aatiaoui A, Koudad M, Chelfi T, Erkan S, Azzouzi M, Aouniti A et al (2021) Experimental and theoretical study of new Schiff bases based on imidazo (1, 2-a) pyridine as corrosion inhibitor of mild steel in 1M HCl. *J Mol Struct* 1226:129372. <https://doi.org/10.1016/j.molstruc.2020.129372>
23. Sayed AR, El-Lateef HMA (2020) Thiocarbonylhydrazones based on adamantane and ferrocene as efficient corrosion Inhibitors for hydrochloric acid pickling of C-steel. *Coatings* 10(11):1068. <https://doi.org/10.3390/coatings10111068>
24. Shenoy KV, Venugopal PP, Kumari PR, Chakraborty D (2021) Effective inhibition of mild steel corrosion by 6-bromo-(2, 4-dimethoxyphenyl) methylidene] imidazo [1, 2-a] pyridine-2-carbohydrazide in 0.5 M HCl: Insights from experimental and computational study. *J Mol Struct* 1232:130074. <https://doi.org/10.1016/j.molstruc.2021.130074>
25. Al-Azawi KF, Mohammed IM, Al-Baghdadi SB, Salman TA, Issa HA, Al-Amiery AA et al (2018) Experimental and quantum chemical simulations on the corrosion inhibition of mild steel by 3-((5-(3, 5-dinitrophenyl)-1, 3, 4-thiadiazol-2-yl) imino) indolin-2-one. *Results Phys* 9:278–283. <https://doi.org/10.1016/j.rinp.2018.02.055>
26. Farj AS, AL-Azawi KF (2022) Synthesis, characterization and antimicrobial activity of novel Mannich bases. *AIP Conf Proc* 2437:020090. <https://doi.org/10.1063/5.0092314>
27. Ozyazici T, Gurdal EE, Orak D, Sipahi H, Ercetin T, Gulcan HO, Koksall M (2020) Synthesis, anti-inflammatory activity, and molecular docking studies of some novel Mannich bases of the 1,3,4-oxadiazole-2(3H)-thione scaffold. *Arch Pharm* 353(7):1–16. <https://doi.org/10.1002/ardp.202000061>
28. Hussain Z, Yousif E, Ahmed A, Altaie A (2014) Synthesis and characterization of Schiff's bases of sulfamethoxazole. *Org Med Chem Lett* 4(1):1. <https://doi.org/10.1186/2191-2858-4-1>
29. Fernandes CM, Alvarez LX, dos Santos NE, Barrios ACM, Ponzio EA (2019) Green synthesis of 1-benzyl-4-phenyl-1H-1, 2, 3-triazole, its application as corrosion inhibitor for mild steel in acidic medium and new approach of classical electrochemical analyses. *Corros Sci* 149:185–194. <https://doi.org/10.1016/j.corsci.2019.01.019>
30. Rashid KH, Khadom AA, Abbas SH (2022) Optimization, kinetics, and electrochemical investigations for green corrosion inhibition of low-carbon steel in 1 M HCl by a blend of onion-garlic leaves wastes. *Bioresour Technol Reports* 19:101194. <https://doi.org/10.1016/j.biteb.2022.101194>
31. Rbaa M, Benhiba F, Dohare P, Lakhrissi L, Tourir R, Lakhrissi B et al (2020) Synthesis of new epoxy glucose derivatives as a non-toxic corrosion inhibitors for carbon steel in molar HCl: experimental, DFT and MD simulation. *Chem Data Collect* 27:100394. <https://doi.org/10.1016/j.cdc.2020.100394>
32. Alkarim TA, Al-Azawi KF, Anaee RA (2021) Anticorrosive properties of Spiramycin for aluminum in acidic medium. *Int J Corros Scale Inhib* 10(3):1168–1188. <https://doi.org/10.17675/2305-6894-2021-10-3-20>
33. El Arrouji S, Karrouchi K, Berisha A, Alaoui KI, Warad I, Rais Z et al (2020) New pyrazole derivatives as effective corrosion inhibitors on steel-electrolyte interface in 1 M HCl: electrochemical, surface morphological (SEM) and computational analysis. *Colloids Surf A Physicochem Eng Aspects* 604:125325. <https://doi.org/10.1016/j.colsurfa.2020.125325>
34. Jasim AS, Rashid KH, AL-Azawi KF, Khadom AA (2022) Synthesis of a novel pyrazole heterocyclic derivative as corrosion inhibitor for low-carbon steel in 1M HCl: characterization, gravimetric, electrochemical, mathematical, and quantum chemical investigations. *Results Eng* 15:100573. <https://doi.org/10.1016/j.RINENG.2022.100573>
35. Saranya J, Sowmiya M, Sounthari P, Parameswari K, Chitra S, Senthilkumar K (2016) N-heterocycles as corrosion inhibitors for mild steel in acid medium. *J Mol Liq* 216:42–52. <https://doi.org/10.1016/j.molliq.2015.12.096>
36. Rashid KH, AL-Azawi KF, Khadom AA, Jasim AS, Kadhim MM (2023) New pyrazole derivative as effective corrosion inhibitor for carbon steel in 1 M HCl: experimental and theoretical analysis. *J Mol Struct*. <https://doi.org/10.1016/j.molstruc.2023.135661>
37. Akinbulumo OA, Odejebi OJ, Odekanle EL (2020) Thermodynamics and adsorption study of the corrosion inhibition of mild steel by *Euphorbia heterophylla* L. extract in 1.5 M HCl. *Results Mater* 5:100074. <https://doi.org/10.1016/j.rinma.2020.100074>
38. Jadaa RJ, Abd AN, Khadom AA (2021) Polyacrylamide as a corrosion inhibitor for mild steel in 2 M phosphoric acid: experimental and theoretical studies. *Chem Pap* 75:5375–5386. <https://doi.org/10.1007/s11696-021-01725-5>

39. Sowmyashree AS, Somya A, Rao S, Kumar CP, Al-Romaizan AN, Hussein MA et al (2023) Potential sustainable electrochemical corrosion inhibition study of Citrus limetta on mild steel surface in aggressive acidic media. *J Market Res* 24:984–994. <https://doi.org/10.1016/j.jmrt.2023.02.039>
40. Fernandes CM, Costa AR, Leite MC, Martins V, Lee HS, da CS Boechat F et al (2023) A detailed experimental performance of 4-quinolone derivatives as corrosion inhibitors for mild steel in acid media combined with first-principles DFT simulations of bond breaking upon adsorption. *J Mol Liq*. <https://doi.org/10.1016/j.molliq.2023.121299>
41. Hajjaji FE, Ech-chihbi E, Salim R, Titi A, Messali M, El Ibrahim B et al (2023) A detailed electronic-scale DFT modeling/MD simulation, electrochemical and surface morphological explorations of imidazolium-based ionic liquids as sustainable and non-toxic corrosion inhibitors for mild steel in 1 M HCl. *Mater Sci Eng, B* 289:116232. <https://doi.org/10.1016/j.mseb.2022.116232>
42. Jasim AS, Khadom AA, Rashid KH, AL-Azawi KF (2022) (3, 5-dimethyl-1H-pyrazol-1-yl)(4-((3, 4-dimethoxybenzylidene)amino) phenyl) methanone as a novel corrosion inhibitor for low-carbon steel in hydrochloric acid: Synthesis, diagnosis, and application. *Results Chem* 4:100569. <https://doi.org/10.1016/j.rechem.2022.100569>
43. Swetha GA, Sachin HP, Guruprasad AM, Prasanna BM, Sudheer Kumar KH (2018) Use of seroquel as an effective corrosion inhibitor for low carbon steel in 1 M HCl. *J Bio Tribo Corros* 4:1–11. <https://doi.org/10.1007/s40735-018-0173-9>
44. Sundaram RG, Vengatesh G, Sundaravivelu M (2021) Surface morphological and quantum chemical studies of some expired drug molecules as potential corrosion inhibitors for mild steel in chloride medium. *Surf Interfaces* 22:100841. <https://doi.org/10.1016/j.surf.2020.100841>
45. Alaoui K, Tourir R, Galai M, Serrar H, Ouakki M, Kaya S et al (2018) Electrochemical and computational studies of some triazepine carboxylate compounds as acid corrosion inhibitors for mild steel. *J Bio Tribo Corros* 4:1–18. <https://doi.org/10.1007/s40735-018-0154-z>
46. El-Hajjaji F, Messali M, Aljuhani A, Aouad MR, Hammouti B, Belghiti ME et al (2018) Pyridazinium-based ionic liquids as novel and green corrosion inhibitors of carbon steel in acid medium: electrochemical and molecular dynamics simulation studies. *J Mol Liq* 249:997–1008. <https://doi.org/10.1016/j.molliq.2017.11.111>
47. Asaad MA, Sarbini NN, Sulaiman A, Ismail M, Huseien GF, Majid ZA, Raja PB (2018) Improved corrosion resistance of mild steel against acid activation: impact of novel *Elaeis guineensis* and silver nanoparticles. *J Ind Eng Chem* 63:139–148. <https://doi.org/10.1016/j.jiec.2018.02.010>
48. Edison TNJI, Atchudan R, Pugazhendhi A, Lee YR, Sethuraman MG (2018) Corrosion inhibition performance of spermidine on mild steel in acid media. *J Mol Liq* 264:483–489. <https://doi.org/10.1016/j.molliq.2018.05.087>
49. Haldhar R, Prasad D, Saxena A, Kumar R (2018) Experimental and theoretical studies of *Ficus religiosa* as green corrosion inhibitor for mild steel in 0.5 M H₂SO₄ solution. *Sustain Chem Pharm* 9:95–105. <https://doi.org/10.1016/j.scp.2018.07.002>
50. Chauhan DS, Ansari KR, Sorour AA, Quraishi MA, Lgaz H, Salghi R (2018) Thiosemicarbazide and thiocarbohydrazide functionalized chitosan as ecofriendly corrosion inhibitors for carbon steel in hydrochloric acid solution. *Int J Biol Macromol* 107:1747–1757. <https://doi.org/10.1016/j.ijbiomac.2017.10.050>
51. Hamani H, Douadi T, Daoud D, Al-Noaimi M, Rikkouh RA, Chafaa S (2017) 1-(4-Nitrophenyl-imino)-1-(phenylhydrazono)-propan-2-one as corrosion inhibitor for mild steel in 1 M HCl solution: weight loss, electrochemical, thermodynamic and quantum chemical studies. *J Electroanal Chem* 801:425–438. <https://doi.org/10.1016/j.jelechem.2017.08.031>
52. Abd El-Lateef HM, Tantawy AH, Abdelhamid AA (2017) Novel quaternary ammonium-based cationic surfactants: synthesis, surface activity and evaluation as corrosion inhibitors for C1018 carbon steel in acidic chloride solution. *J Surfactants Deterg* 20:735–753. <https://doi.org/10.1007/s11743-017-1947-7>
53. Salhi A, Tighadouini S, El-Massaoudi M, Elbelghiti M, Bouyanzer A, Radi S et al (2017) Keto-enol heterocycles as new compounds of corrosion inhibitors for carbon steel in 1 M HCl: weight loss, electrochemical and quantum chemical investigation. *J Mol Liq* 248:340–349. <https://doi.org/10.1016/j.molliq.2017.10.040>
54. Yan Y, Lin X, Zhang L, Zhou H, Wu L, Cai L (2017) Electrochemical and quantum-chemical study on newly synthesized triazoles as corrosion inhibitors of mild steel in 1 M HCl. *Res Chem Intermed* 43:3145–3162. <https://doi.org/10.1007/s11164-016-2816-0>
55. Nathiya RS, Perumal S, Moorthy M, Murugesan V, Rangappan R, Raj V (2020) Synthesis, characterization and inhibition performance of Schiff bases for aluminium corrosion in 1 M H₂SO₄ solution. *J Bio Tribo Corros* 6:1–15. <https://doi.org/10.1007/s40735-019-0291-z>
56. Haque J, Srivastava V, Verma C, Quraishi MA (2017) Experimental and quantum chemical analysis of 2-amino-3-((4-(S)-2-amino-2-carboxyethyl)-1H-imidazol-2-yl) thio) propionic acid as new and green corrosion inhibitor for mild steel in 1 M hydrochloric acid solution. *J Mol Liq* 225:848–855. <https://doi.org/10.1016/j.molliq.2016.11.011>
57. Anusuya N, Saranya J, Sounthari P, Zarrouk A, Chitra S (2017) Corrosion inhibition and adsorption behaviour of some bispyrimidine derivatives on mild steel in acidic medium. *J Mol Liq* 225:406–417. <https://doi.org/10.1016/j.molliq.2016.11.015>
58. Salarvand Z, Amirnasr M, Talebian M, Raeissi K, Meghdadi S (2017) Enhanced corrosion resistance of mild steel in 1 M HCl solution by trace amount of 2-phenyl-benzothiazole derivatives: experimental, quantum chemical calculations and molecular dynamics (MD) simulation studies. *Corros Sci* 114:133–145. <https://doi.org/10.1016/j.corsci.2016.11.002>
59. Hameed WF, Rashid KH, Khadom AA (2022) Investigation of tetraazaadamantane as corrosion inhibitor for mild steel in oilfield produced water under sweet corrosive environment. *J Bio Tribo Corros* 8(1):27. <https://doi.org/10.1007/s40735-021-00626-0>
60. Laggoun R, Ferhat M, Saidat B, Benghia A, Chaabani A (2020) Effect of p-toluenesulfonyl hydrazide on copper corrosion in hydrochloric acid solution. *Corros Sci* 165:108363. <https://doi.org/10.1016/j.corsci.2019.108363>
61. Xu B, Yang W, Liu Y, Yin X, Gong W, Chen Y (2014) Experimental and theoretical evaluation of two pyridinecarboxaldehyde thiosemicarbazone compounds as corrosion inhibitors for mild steel in hydrochloric acid solution. *Corros Sci* 78:260–268. <https://doi.org/10.1016/j.corsci.2013.10.007>
62. Wang X, Yang H, Wang F (2011) An investigation of benzimidazole derivative as corrosion inhibitor for mild steel in different concentration HCl solutions. *Corros Sci* 53(1):113–121. <https://doi.org/10.1016/j.corsci.2010.09.029>
63. Goyal M, Kumar S, Bahadur I, Verma C, Ebenso EE (2018) Organic corrosion inhibitors for industrial cleaning of ferrous and non-ferrous metals in acidic solutions: a review. *J Mol Liq* 256:565–573. <https://doi.org/10.1016/j.molliq.2018.02.045>
64. Singh P, Quraishi MA, Gupta SL, Dandia A (2016) Investigation of the corrosion inhibition effect of 3-methyl-6-oxo-4-(thiophen-2-yl)-4,5,6,7-tetrahydro-2H pyrazolo [3,4-b]pyridine-5-carbonitrile (TPP) on mild steel in hydrochloric acid. *J Taibah Univ Sci* 10:139–147. <https://doi.org/10.1016/j.jtusc.2015.07.005>

Publisher's Note Springer Nature remains neutral with regard to jurisdictional claims in published maps and institutional affiliations.

Springer Nature or its licensor (e.g. a society or other partner) holds exclusive rights to this article under a publishing agreement with the

author(s) or other rightsholder(s); author self-archiving of the accepted manuscript version of this article is solely governed by the terms of such publishing agreement and applicable law.